

Statistical Uncertainties of Limit Cycle Systems in Langevin Bath

Dipesh K. Singh and P. K. Mohanty*

Department of Physical Sciences, Indian Institute of Science Education and Research Kolkata, Mohanpur, 741246, India.

(Dated: February 19, 2025)

We show that limit cycle systems in Langevin bath exhibit uncertainty in observables that define the limit-cycle plane, and maintain a positive lower bound. The uncertainty-bound depends on the parameters that determine the shape and periodicity of the limit cycle. In one dimension, we use the framework of canonical dissipative systems to construct the limit cycle, whereas in two dimensions, particle in central potentials with radial-dissipation provide us natural examples. We show that, the position-momenta uncertainty of particle in a central potential is larger than half the magnitude of the angular momentum (conserved) of the particle. We also investigate how uncertainties, which are absent in deterministic systems, increase with time when the systems are attached to a bath and eventually cross the lower bound before reaching the steady state.

I. INTRODUCTION

A limit cycle is a closed trajectory in the phase space of a dynamical system [1, 2], and its stability depends on whether neighboring trajectories approach the limit cycle as time progresses. Limit cycle (LC) systems are abundant in nature and play a fundamental role in predicting and studying self-sustained oscillations observed across various scientific disciplines, such as neuroscience [3, 4], ecology [5, 6], electrical engineering [7], and chemical systems [8, 9]. Ranging from the Hodgkin-Huxley model [10] that demonstrates how neurons exhibit rhythmic firing patterns, periodic population fluctuations in predator-prey dynamics [11] described by the Lotka-Volterra equations, application of van der Pol oscillators [12] in radio frequency applications, aircraft wing-fluttering [13] and nonlinear oscillations in electrical circuits [7], limit cycle oscillations play a key role. The emergence of stable limit cycles is an essential phenomenon that sustains life on Earth [14]: beating of the heart, the circadian rhythms, regulation of biological pathways, planetary and climate cycles are oscillatory processes, and their emergence and stability are essential in the continuity of life-processes.

Stability of LCs to different kind of perturbations and noise has been a question of importance for decades [15–17]. Nonlinearity, which is responsible for giving birth to LCs can also destroy them [2]. The effect of noise is usually destructive; small amount of noise can produce irregular LCs with trajectories not so far away from the original LC curve, whereas strong noise can destroy the LC behaviour [15–17]. Coupled limit cycle systems may exhibit entrainment in presence of noise [18]. A recent study shows that moderate noise on a limit cycle oscillator can produce counterrotation and bistability [19].

In this article, we show that Limit cycle systems in Langevin bath exhibit unusual residual fluctuations that survive in the zero-noise limit. As a consequence position-momenta uncertainties, i.e., a positive lower bound in $\Delta x \Delta p_x$, is observed when limit cycles are

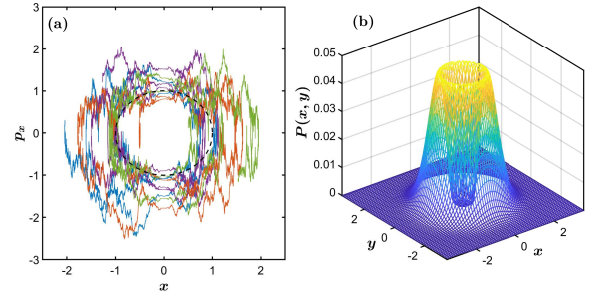


FIG. 1. (a) Sample paths starting from four different initial conditions for the 2D simple harmonic oscillator limit cycle for $k = \ell = 1$ and $\gamma = 2$ at $T = 0.5$ in the x - p_x plane. The limit cycle is marked by the dashed lines. (b) Steady state distribution in the x - y plane.

formed in x - p_x phase plane. The lower-bound depends on the parameters that control the size and shape of the limit cycle and the time required for the system to complete one cycle. For a large set of central potentials in two dimensions, with conserved angular momentum ℓ , we find that $\Delta x \Delta p_x \geq \frac{|\ell|}{2}$.

In Fig. 1 we demonstrate these results for a simple harmonic oscillator (SHO) in two dimension (2D) in presence of a radial Langevin bath at temperature T , that keeps the angular momentum ℓ conserved. The steady state marginal distribution $P(x, y)$, shown in Fig. 1, is centered around the curve $x^2 + y^2 = r_c^2$; the noisy circular motion about this curve in real space translates to similar motion in x - p_x phase plane resulting in a position momenta uncertainty relation $\Delta x \Delta p_x \geq |\ell|/2$.

Thermodynamic uncertainty relations [20, 21] or statistical bounds [22] are not new to statistical physics, but their presence in limit cycle systems is rather surprising. It is interesting to note that some of the features of a two dimensional harmonic oscillator in the presence of a moderate thermal noise is quite similar to what one observes in the corresponding quantum system. In particular, we find that the position-momentum uncertainty bound is proportional to the conserved angular momentum of the system and the position autocorrelation at

* pkmohanty@iiserkol.ac.in

low temperature exhibits sinusoidal oscillations.

The article is organized as follows: we start with one dimensional systems in Sec. II, highlighting a way of generating limit cycles by modifying Hamiltonian dynamics in Sec. II A and introduce the notion of uncertainty using an example in Sec. II B. We move on to two dimensional systems in Sec. III where we define a method of generating limit cycles using central potentials (Sec. III A) and show the existence of uncertainty relations. We then elucidate this general framework by considering some examples in Secs. III B and III C. We finally highlight the dynamical features of these systems via numerical simulation in Sec. IV followed by a rich discussion in Sec. V. The conclusion with a few remarks are given in Sec. VI.

II. LIMIT CYCLES IN ONE DIMENSIONAL SYSTEMS

Time independent Hamiltonian systems in one dimension (1D) with added linear damping cannot produce limit cycles in the x - p_x phase plane. In this section, we utilize the framework of canonical dissipative systems [23–25] to modify Hamiltonian dynamics which yields limit cycles, and show the presence of position-momentum uncertainties.

A. Constructing Limit Cycles

Any Hamiltonian, $H(x, p_x)$, which produces closed orbits given by $H = E_0$ in the x - p_x phase space can be used to construct limit cycles in the same phase space under the framework of canonical dissipative systems. We then use a Langevin-like bath. The noisy dynamics of the limit cycle oscillator is described by

$$\dot{x} = \frac{\partial H}{\partial p_x}, \quad \dot{p}_x = -\frac{\partial H}{\partial x} - \gamma g(H) \frac{\partial H}{\partial p_x} + \sqrt{\gamma T} \xi(t) \quad (1)$$

where $\gamma > 0$ and $\xi(t)$ is a Gaussian white noise with $\langle \xi(t) \rangle = 0$ and $\langle \xi(t) \xi(t') \rangle = 2\delta(t-t')$. We use units where mass and Boltzmann constant are unity ($m = k_B = 1$). A non-decreasing function $g(H)$, with appropriate dimension, is chosen such that $g(H) = 0$ describes a closed curve in the phase space. Then, in absence of noise (at $T = 0$) the above system sustains limit cycle oscillations, whose equation in the phase space is given by $g(H) = 0$. The steady state Fokker-Planck equation can be written as (see Supplemental Material [26] for details)

$$[H, P] + \frac{\partial}{\partial p_x} \left(\gamma g(H) \frac{\partial H}{\partial p_x} P + \gamma T \frac{\partial P}{\partial p_x} \right) = 0 \quad (2)$$

where $[H, P] = \frac{\partial H}{\partial x} \frac{\partial P}{\partial p_x} - \frac{\partial H}{\partial p_x} \frac{\partial P}{\partial x}$ is the Poisson bracket of H and P . The above equation is easily solved using the ansatz $P = P(H)$ leading to a steady state distribution

$$P(x, p_x) = \frac{1}{Z} \exp \left(-\beta \int dH(x, p_x) g(H(x, p_x)) \right) \quad (3)$$

where $\beta \equiv T^{-1}$ and Z is the partition function,

$$Z(\beta) = \int_{-\infty}^{\infty} dp_x \int_{-\infty}^{\infty} dx \exp \left(-\beta \int dH g(H) \right). \quad (4)$$

The validity of the distribution requires the probability density integrated over all space, that is, the partition function Z , to be finite.

For the simplest $g(H)$ possible, that is, a function linear in H , given by $g(H) = H/E_0 - 1$, $E_0 > 0$. In the absence of noise (at $T = 0$), this system produces a limit cycle whose equation in the phase space is given by $H = E_0$. The solution of the Fokker-Planck equation leads to a steady state distribution

$$P(x, p_x) = \frac{1}{Z_{E_0}} \exp \left(-\frac{\beta}{2E_0} (H(x, p_x) - E_0)^2 \right), \quad (5)$$

which is a valid probability density function (PDF) if Z_{E_0} is finite.

Here, the inhomogeneous dissipation creates a nonequilibrium bath leading to a steady state that differs from Boltzmann distribution with respect to H ; T being only a parameter of the bath, need not be treated as temperature. Such a nonequilibrium bath is a necessity in one dimension, where linear damping cannot generate a limit cycle.

B. Limit Cycle construction using 1D Simple Harmonic Oscillator

We consider one of the simplest Hamiltonian systems, a one dimensional simple harmonic oscillator, described by the Hamiltonian, $H = p_x^2/2 + kx^2/2$, with frequency $\omega_0 = \sqrt{k}$. It produces elliptical orbits in the x - p_x phase space. We also choose $g(H) = H/E_0 - 1$, $E_0 > 0$. The noisy dynamics of the limit cycle oscillator is described according to (1),

$$\dot{x} = p_x, \quad \dot{p}_x = -kx - \gamma \left(\frac{H}{E_0} - 1 \right) p_x + \sqrt{\gamma T} \xi(t). \quad (6)$$

As expected, in the absence of noise (at $T = 0$) the above system produces an elliptical limit cycle whose equation in the phase space is given by $H = E_0$. The solution of the Fokker-Planck equation corresponding to the Langevin dynamics in Eq. (6) leads to a steady state distribution given by Eq. (5),

$$P(x, p_x) = \frac{1}{Z_{E_0}} \exp \left(-\frac{\beta}{2E_0} \left(\frac{p_x^2 + kx^2}{2} - E_0 \right)^2 \right), \quad (7)$$

with the partition function, Z_{E_0} (see Supplemental Material [26] for detailed calculation),

$$Z_{E_0}(\beta) = \sqrt{\frac{2E_0}{k\beta}} \pi^{3/2} \left(1 + \operatorname{erf} \left(\sqrt{\beta E_0/2} \right) \right). \quad (8)$$

Let's proceed to calculate the moments. As expected $\langle x \rangle = 0 = \langle p_x \rangle$, and

$$k \langle x^2 \rangle = \langle p_x^2 \rangle = \langle H \rangle = E_0 + \frac{e^{-\beta E_0/2} \sqrt{2E_0/\pi\beta}}{1 + \operatorname{erf}\left(\sqrt{\beta E_0/2}\right)}. \quad (9)$$

Now we turn our attention to the uncertainty, which is defined for an observable O as $\Delta O \equiv \sqrt{\langle O^2 \rangle - \langle O \rangle^2}$; in steady state we get,

$$\Delta x \Delta p_x = \frac{1}{\omega_0} \left(E_0 + \frac{e^{-\beta E_0/2} \sqrt{2E_0/\pi\beta}}{1 + \operatorname{erf}\left(\sqrt{\beta E_0/2}\right)} \right) \quad (10)$$

which does not vanish in the $T \rightarrow 0$ limit, leading to a position-momentum uncertainty relation,

$$\Delta x \Delta p_x \geq \frac{E_0}{\omega_0}. \quad (11)$$

The equality holds only in the limiting sense, that is, as $T \rightarrow 0$. Note that $\langle H \rangle (T \rightarrow 0) = E_0$, which is the equation of the limit cycle in the x - p_x plane (phase space).

We claim that such uncertainty relations are common to limit cycle systems in Langevin bath. We shall always have some uncertainty relation whenever there is a limit cycle in any two dimensional projection of phase space. To study higher dimensional systems, the formalism in Sec. II A can of course be extended, but the set of equations do not guarantee a limit cycle at $H = E_0$ in higher dimensions [25]. We present a simple way of creating limit cycles in two dimensions and highlight its features under noise.

III. LIMIT CYCLES IN TWO DIMENSIONAL SYSTEMS

In 1D, we have shown the presence of uncertainty in the conjugates (x, p_x) . However, we had to introduce a nonlinear dissipation in momentum to obtain the limit cycle. This in turn produced a nonequilibrium bath. The uncertainty relation however, is not a consequence of the nonequilibrium bath. We illustrate this for a particle experiencing a central potential $V(r)$ in two dimension, in presence of a usual equilibrium/Langevin bath.

A. Particle in a Central Potential

Consider the Hamiltonian in two dimension, with coordinates (r, ϕ) and momenta (p_r, p_ϕ) ,

$$H = \frac{p_r^2}{2} + \frac{p_\phi^2}{2r^2} + V(r). \quad (12)$$

Since p_ϕ is cyclic, the angular momentum $p_\phi = \ell$ is conserved. We use a radial Langevin bath which respects

this conservation law. The equations of motion are now given by

$$\dot{r} = p_r; \dot{p}_r = -V'(r) + \frac{\ell^2}{r^3} - \gamma p_r + \sqrt{\gamma T} \xi(t); \dot{\phi} = \frac{\ell}{r^2}, \quad (13)$$

where prime denotes derivative with respect to r . In absence of noise ($T = 0$) and $\ell \neq 0$, the radial equation produces stable (unstable) limit cycle in x - y plane at $r = \sqrt{x^2 + y^2} = r_c$, where r_c is the minimum (maximum) of the effective radial potential, $\tilde{V}(r) = \ell^2/2r^2 + V(r)$. In effect, stable or unstable limit cycles are also produced in p_x - p_y , x - p_x and y - p_y planes with the equations

$$p_x^2 + p_y^2 = \frac{\ell^2}{r_c^2}, \quad \frac{x^2}{r_c^2} + \frac{r_c^2 p_x^2}{\ell^2} = 1, \quad \frac{y^2}{r_c^2} + \frac{r_c^2 p_y^2}{\ell^2} = 1. \quad (14)$$

For any $T \neq 0$, the Fokker-Planck equation corresponding to the Langevin dynamics (13) is

$$[H, P] + \frac{\partial}{\partial p_r} \left(\gamma p_r P + \gamma T \frac{\partial P}{\partial p_r} \right) = 0 \quad (15)$$

and admits a steady state given by the Boltzmann distribution $P(r, p_r, p_\phi = \ell) = \frac{e^{-\beta H}}{\mathcal{Z}_\ell(\beta)}$, where the partition function is

$$\mathcal{Z}_\ell(\beta) = 2\pi \sqrt{\frac{2\pi}{\beta}} \int_0^\infty dr \exp\left(-\beta \left(\frac{\ell^2}{2r^2} + V(r)\right)\right). \quad (16)$$

Of course, $\mathcal{Z}_\ell(\beta)$ must be finite, as required for a valid probability density function (see Supplemental Material [26] for details).

From the symmetries of the Hamiltonian, it is clear that $\langle x^n \rangle = \langle y^n \rangle$, $\langle p_x^n \rangle = \langle p_y^n \rangle \forall n$ and they vanish when n is odd. Further, $\langle x^2 \rangle = \frac{1}{2} \langle r^2 \rangle$ and from the relations $\frac{1}{2} \langle p_x^2 + p_y^2 \rangle = \frac{1}{2} \langle p_r^2 + \frac{\ell^2}{r^2} \rangle$ and $\frac{1}{2} \langle p_r^2 \rangle = T/2$, we get $\langle p_x^2 \rangle = \frac{1}{2} (T + \ell^2 \langle \frac{1}{r^2} \rangle)$. Therefore,

$$\Delta x \Delta p_x = \Delta y \Delta p_y = \frac{1}{2} \sqrt{\langle r^2 \rangle (T + \ell^2 \langle 1/r^2 \rangle)}. \quad (17)$$

Provided both $\langle r^2 \rangle$ and $\langle \frac{1}{r^2} \rangle$ are finite, the Cauchy-Schwarz inequality ensures $\langle r^2 \rangle \langle 1/r^2 \rangle \geq 1$ and then Eq. (17) leads us to the uncertainty relations,

$$\Delta x \Delta p_x = \Delta y \Delta p_y \geq \frac{|\ell|}{2}. \quad (18)$$

Here, the equality holds in the limit $T \rightarrow 0$. From the above relations, it is clear there are positive lower bounds in each of the quantities, Δx , Δy , Δp_x and Δp_y .

At small T , we calculate the radial moments using saddle-point approximation (see Supplemental Material [26] for calculation) and find that in $T \rightarrow 0$ limit $\langle r \rangle = r_c$ and $\langle r^n \rangle = \langle r \rangle^n \forall n \geq 0$. Thus, certainly the particle remains on the limit cycle as $T \rightarrow 0$, having a residual energy $\langle E \rangle = E_c$. Fluctuations in r and E vanish in this limit, but the uncertainty relation (18) holds.

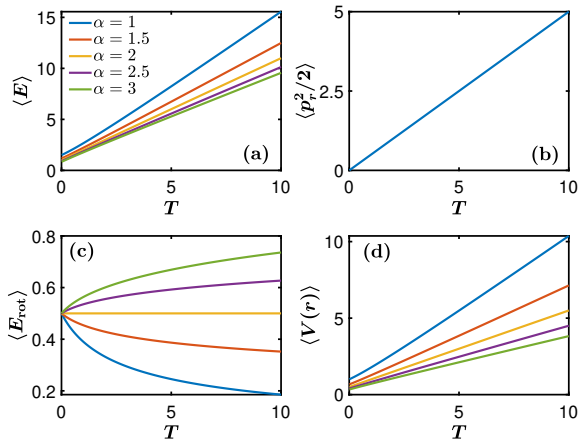


FIG. 2. Variation of average energy, $\langle E \rangle = \langle p_r^2/2 \rangle + \langle E_{\text{rot}} \rangle + \langle V(r) \rangle$ with T for $\alpha = 1, 1.5, 2, 2.5, 3$. We choose $k = \ell = 1$, hence, $r_c = 1$. (a) shows the increase of $\langle E \rangle$ with T . The growth is faster for smaller α and $\langle E \rangle(T \rightarrow 0) = E_c = (2 + \alpha)/2\alpha$. (b) $\langle p_r^2/2 \rangle = T/2$ for all values of α . (c) $\langle E_{\text{rot}} \rangle$ decreases for $\alpha < 2$, is constant for $\alpha = 2$ and increases for $\alpha > 2$. (d) $\langle V(r) \rangle$ always increases with T with a more rapid increase for smaller values of α . Exact expressions are given in Supplemental Material [26].

B. Example I: Power Law Potentials

As an example, let us consider the potentials

$$V(r) = \frac{kr^\alpha}{\alpha}; \quad k, \alpha > 0 \quad (19)$$

which yield the integral in (16) finite. Note that, limit cycles are generated at $T = 0$ even for potentials with $\alpha \in (-2, 0)$ but under noise, the resulting steady state PDF does not converge on integration over all space. Thus, we restrict ourselves to $\alpha > 0$ case.

In the absence of noise ($T = 0$) the particle is attracted to a limit cycle trajectory in the x - y plane having radius r_c and energy E_c , given by

$$r_c = \left(\frac{\ell^2}{k}\right)^{\frac{1}{\alpha+2}}, \quad E_c = k \left(\frac{2+\alpha}{2\alpha}\right) r_c^\alpha \quad (20)$$

Apart from the uncertainty bound, these systems also exhibit interesting behaviour in the variation of average energy with temperature. $\langle p_r^2/2 \rangle = T/2$ for all α and $\langle E \rangle$ is an increasing function of T with $\langle E \rangle(T \rightarrow 0) = E_c$ as expected but the average rotational kinetic energy, $\langle E_{\text{rot}} \rangle = \langle \ell^2/2r^2 \rangle$ is a decreasing function of T vanishing as $T \rightarrow \infty$ for $\alpha \in (0, 2)$, a constant with value equal to $\frac{1}{2}\sqrt{k}|\ell|$ for $\alpha = 2$ and for $\alpha > 2$, an increasing function of T going to infinity as $T \rightarrow \infty$. However, for any α , we have $\langle E_{\text{rot}} \rangle(T \rightarrow 0) = \ell^2/2r_c^2$. Figure 2 shows the variation of average energy with T for different α .

C. Example II: Logarithmic Potential

Another interesting example is the case of the logarithmic potential,

$$V(r) = k \ln\left(\frac{r}{r_0}\right); \quad k, r_0 > 0 \quad (21)$$

At $T = 0$, the above potential has a limit cycle at r_c and energy E_c , given by

$$r_c = \left(\frac{\ell^2}{k}\right)^{1/2}, \quad E_c = \frac{k}{2} \left(1 + \ln\left(\frac{\ell^2}{kr_0^2}\right)\right) \quad (22)$$

For $T \neq 0$, the Fokker-Planck equation has a steady state $\mathcal{Z}_\ell(\beta)^{-1} e^{-\beta H}$ only when $k\beta > 1$, as

$$\mathcal{Z}_\ell(\beta) = \left(r_0 \sqrt{\frac{2}{\beta}}\right)^{k\beta} \pi^{3/2} |\ell|^{1-k\beta} \Gamma\left(\frac{k\beta-1}{2}\right) \quad (23)$$

converges only for $k\beta > 1$. The n -th radial moment exists only when $k\beta > n + 1$ given by

$$\langle r^n \rangle = \left(\frac{\beta}{2}\right)^{n/2} |\ell|^n \frac{\Gamma\left(\frac{k\beta-n-1}{2}\right)}{\Gamma\left(\frac{k\beta-1}{2}\right)}. \quad (24)$$

In this case, for $T \geq k/3$, $\langle r^2 \rangle$ and hence $\langle x^2 \rangle = \langle y^2 \rangle$ do not exist and we cannot talk about uncertainties. The uncertainty relation (18) definitively holds for $T < k/3$ and as $T \rightarrow 0$, Δr and ΔE vanish.

IV. DYNAMICAL UNCERTAINTY

All the inequalities we talked about in this article hold in the steady state. Therefore, we must have, dynamically, a time scale t^* such that the uncertainty relations become valid for all times $t > t^*$.

The system evolves deterministically at $T = 0$, where the position and momenta of the particle at any time t depend on the initial condition; such deterministic trajectories result in $\Delta x(t) = 0 = \Delta p_x(t)$. One can, however, choose an ensemble of particles with initial condition distributed according to some arbitrary PDF to get a non-zero variance of x (and y, p_x, p_y) that depends on the choice of initial PDF. The situation for $T \neq 0$ is different. Non-zero T introduces noise to the dynamics, leading the system to a unique steady state, independent of initial conditions.

Naturally, in the initial state, all degrees of freedom x, y, p_x, p_y are uncorrelated; thus, $\Delta x \Delta p_x$ can be made arbitrarily small at $t = 0$. We consider a fixed initial value $(x, y, p_x, p_y) = (x_0, y_0, p_{x0}, p_{y0})$ so that $\Delta x = 0 = \Delta p_x$ at $t = 0$ and follow the dynamics to find out how $\Delta x \Delta p_x$ increases as time progresses and crosses the uncertainty bound $|\ell|/2$ at $t = t^*$ before the system reaches its steady state. For small T , the steady state value of $\Delta x \Delta p_x$ is

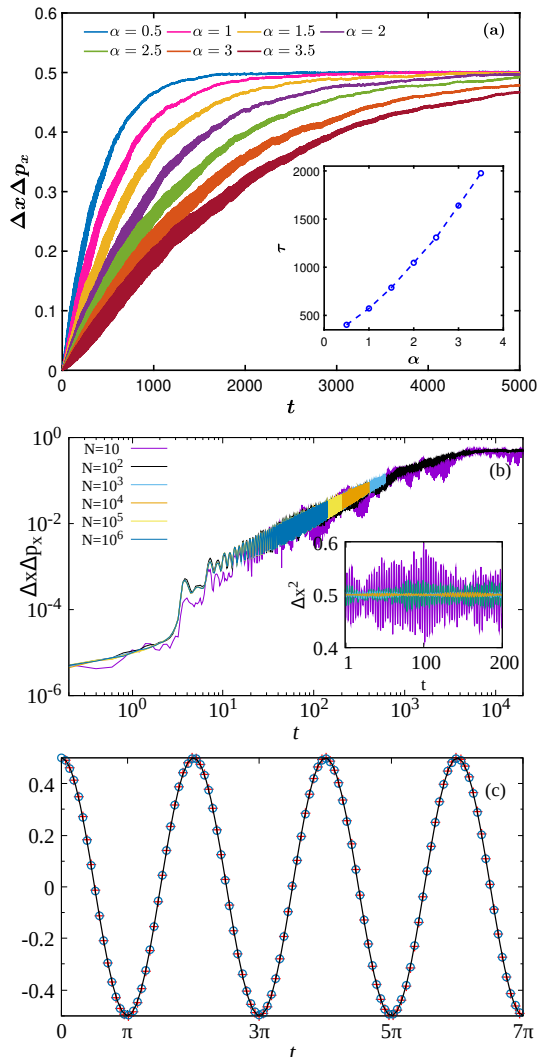


FIG. 3. (a) Variation of $\Delta x \Delta p_x$ with t for $\alpha = 0.5, 1, 1.5, 2, 2.5, 3, 3.5$, $\gamma = 2$, $k = 1 = \ell$ at $T = 10^{-3}$. The inset shows the relaxation time τ as a function of α . (b) Evolution of $\Delta x \Delta p_x$, when averaged over N samples. The large oscillations observed at small t are characteristic features of the dynamics; they are robust, and do not disappear even after averaging over $N = 10^6$ samples. The inset shows steady state oscillations; the amplitude of the oscillations reduces as the number of samples increase. (c) The steady state average of the autocorrelation functions $\langle x(0)x(t) \rangle$ (dots) and $\langle y(0)y(t) \rangle$ (crosses) are compared with $\cos(\omega t)$. $T = 10^{-3}$, $\alpha = 2$, $\gamma = k = \ell = 1$. Thus, $r_c = 1$ and $\omega = \ell/r_c^2 = 1$.

slightly higher than $|\ell|/2$ and thus one expects $t^* \sim \tau$, the time of relaxation to steady state.

In Fig. 3(a) we show the evolution of $\Delta x \Delta p_x$ for a particle experiencing a central potential $V(r) = \frac{k r^\alpha}{\alpha}$. We keep the temperature very low, $T = 10^{-3}$, and study the evolution for different α . With an initial condition having angular momentum $\ell = 1$, one expect $\Delta x \Delta p_x \geq \frac{1}{2}$. It is evident from Fig. 3(a) that, $\Delta x \Delta p_x$ approaches

this bound as $t \rightarrow \infty$. Initially at small t , the curves appear thicker - this might give an impression that the data is not averaged enough. However, for such a low temperature, the trajectory of the particle in x - p_x plane is not far away from the limit cycle, and most observables exhibit sustained oscillations. As illustrated in Fig. 3(b) for $\alpha = 2$, the oscillations are in fact the property of the system and not a numerical artifact of inadequate ensemble averaging. These oscillations do survive in the steady state. Their amplitude however decreases as one increase the sample size N ; this is shown in the inset of Fig. 3(b). From the log-scale plot of $\Delta x \Delta p_x - \frac{|\ell|}{2}$ as a function of t we obtain the relaxation time τ ; a plot of τ vs α is shown in the inset of Fig. 3(a). For larger α , one may naively expect the system to relax faster as the potential-confinement is tighter. However, we find that the relaxation time increases with α , owing to the inertia of the particle. For larger α , the particle lands near the LC with a high velocity and goes farther away to the other side of the LC, creating oscillations, which survive longer for larger α . In fact, the dissipation strength γ controls how fast the system reaches near the LC $r = r_c$. A linear stability analysis about r_c (at $T = 0$) shows that the relaxation time of r and p_r is $\tau_r = 2/\gamma$; we find the time scale for relaxation of $\langle r \rangle$ and $\langle p_r \rangle$ to be $\simeq \tau_r$ when T is small (see Supplemental material [26] for details). On the other hand, oscillations one sees in $\langle x \rangle$, $\langle y \rangle$ and $\langle p_{x,y} \rangle$ are controlled by the temperature T which could not be captured from the linear stability analysis at $T = 0$, reconfirming the fact that the system at any T , however small it may be, cannot be treated as a perturbation to the deterministic dynamics at $T = 0$.

The oscillatory nature of the steady state at finite T can also be seen from the autocorrelation functions $C_x(t) = \langle x(0)x(t) \rangle$ and $C_y(t) = \langle y(0)y(t) \rangle$, which are shown in Fig. 3(c) for $\alpha = 2$ (SHO). We find that $C_x(t) = \cos t = C_y(t)$ both having a period of 2π , which can be explained as follows. Since $\langle r \rangle$ relaxes very quickly to r_c , we can safely assume $r = r_c$ in the steady state. Thus $x(t) \sim r_c \cos(\omega t + \phi)$ and $y(t) \sim r_c \sin(\omega t + \phi)$, with initial position of the particle $(x(0), y(0)) = (r_c \cos \phi, r_c \sin \phi)$. When averaged over the initial condition, we get

$$\langle x(0)x(t) \rangle = \frac{r_c^2}{2\pi} \int_0^{2\pi} d\phi \cos(\omega t + \phi) \cos(\phi) = \frac{r_c^2}{2} \cos(\omega t)$$

which is same as $\langle y(0)y(t) \rangle$, as observed in Fig. 3(c).

V. DISCUSSION

A. Uncertainties without Limit Cycle

As illustrated in Sec. III, the uncertainty relations are not a consequence of the nonequilibrium bath. In Sec. II A, we encountered a steady state, non-Boltzmann in H . However, these nonequilibrium steady states can be equilibrium steady states of another dynamics which may

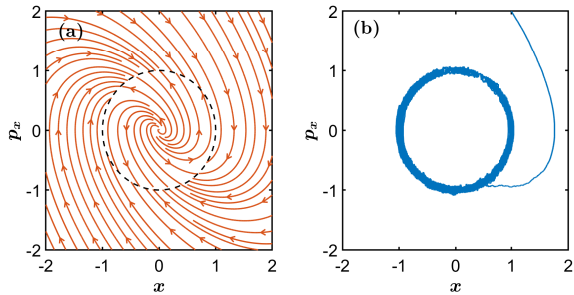


FIG. 4. (a) Flow generated by the system of equations (30) for $E_0 = 0.5, \gamma = 1 = k$. The ellipse (here, circle) of fixed points $H = E_0$ is shown by dashed lines (b) A sample path of the dynamics (30) at $T = 10^{-3}$ with $\gamma = 1 = k$ and $E_0 = 0.5$.

not necessarily generate limit cycles at $T = 0$ but they may behave like a limit cycle system when $T \neq 0$. These systems are expected to show uncertainty relations. We illustrate this by devising an alternate dynamics which will generate the same steady state as (3) but may not produce a limit cycle.

We define an auxiliary Hamiltonian, \tilde{H} , corresponding to H in (3) as

$$\tilde{H} = \int dH g(H). \quad (25)$$

Consider the dynamics (see Supplemental Material [26] for details on constructing the dynamics)

$$\dot{x} = \frac{\partial \tilde{H}}{\partial p_x}, \quad \dot{p}_x = -\frac{\partial \tilde{H}}{\partial x} - \gamma \frac{\partial \tilde{H}}{\partial p_x} + \sqrt{\gamma T} \xi(t). \quad (26)$$

The steady state Fokker-Planck equation for the above dynamics reads as

$$\left[\tilde{H}, P \right] + \frac{\partial}{\partial p_x} \left(\gamma \frac{\partial \tilde{H}}{\partial p_x} P + \gamma T \frac{\partial P}{\partial p_x} \right) = 0, \quad (27)$$

which leads to the steady state distribution

$$P(x, p_x) = \frac{1}{\mathcal{Z}} \exp\left(-\beta \tilde{H}(x, p_x)\right). \quad (28)$$

Here, \mathcal{Z} is given by Eq. (4). We proceed with $H = p_x^2/2 + kx^2/2$, the Hamiltonian of a 1D SHO considered in Sec. II B with

$$\tilde{H}(x, p_x) = \frac{(H(x, p_x) - E_0)^2}{2E_0}. \quad (29)$$

The dynamics according to (26) is

$$\dot{x} = \frac{p_x}{E_0} (H - E_0); \quad \dot{p}_x = -\left(\frac{H - E_0}{E_0}\right) (kx + \gamma p_x) + \sqrt{\gamma T} \xi(t) \quad (30)$$

At $T = 0$, the above system has an ellipse of fixed points at $H = E_0$ shown in Fig. 4 (a) and produces no limit

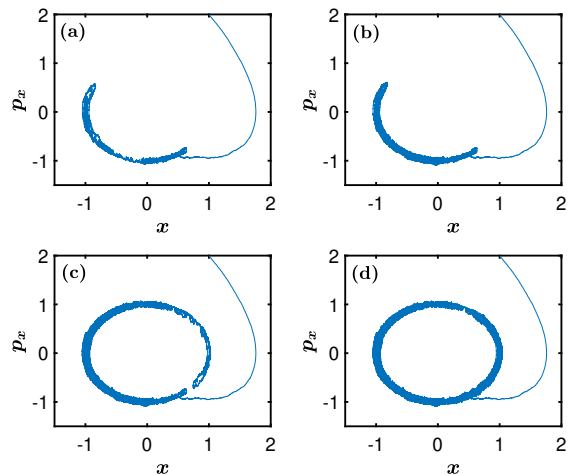


FIG. 5. The particle starts from the initial condition (1, 2) at $T = 10^{-3}$ with $\gamma = k = 1$ and $E_0 = 0.5$ (a) Snapshot of the trajectory at $t = 400$. The particle has moved clockwise around the ellipse of fixed points (b) Snapshot at $t = 1400$. The particle has moved back anticlockwise over the ellipse of fixed points as indicated by the increased line density of plot. (c) Snapshot at $t = 3800$. The particle has moved clockwise again, almost covering completely the ellipse of fixed points. (d) Snapshot at $t = 5000$. The particle has covered fully the ellipse of fixed points, however, the increased line density in the plot is a signature of the particle moving repeatedly clockwise as well as anticlockwise over the ellipse of fixed points.

cycle. Nevertheless, at non-zero T , it is described by the steady state (28) with \tilde{H} as defined in (29) and the uncertainty relation (11) holds.

As can be seen in Fig. 4 (b), under weak noise, the particle moves over the ellipse of fixed points as expected from the steady state distribution. However, the motion is quite different from a limit cycle system where the noisy trajectories are definitively clockwise or anticlockwise depending on the direction of rotation of the particle in the limit cycle at $T = 0$. In the system considered here, the noisy trajectories are about the ellipse of fixed points but have no directional preference. This is illustrated in Fig. 5.

As a result, the oscillatory behaviour in the position-momentum moments as well as the position-momentum uncertainty highlighted in Sec. IV is not exhibited in this system. The $(\Delta x \Delta p_x)(t)$ generated by dynamics (30) is compared with the dynamics given in Eq. (6) for $\gamma = k = 1$ at $T = 10^{-3}$ in Fig. 6.

B. Origin of uncertainty bound

It is true, at least mathematically, that the uncertainty relations are simply features of some specific probability distributions. If a stochastic variable z has a normal distribution with mean z_c and standard deviation σ ,

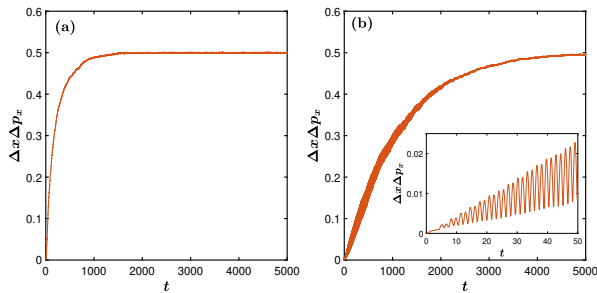


FIG. 6. (a) and (b) show $\Delta x \Delta p_x$ as a function of t for dynamics (30) and (6) respectively. The simulations have been performed at $T = 10^{-3}$ for $\gamma = k = 1$ and $E_0 = 0.5$. At low noise, the uncertainties roughly hold the equality in the uncertainty relation (11) and approach $E_0/\omega_0 = 0.5$. In (b), the system has a limit cycle at $T = 0$ and hence, the oscillatory behaviour shown in the inset as opposed to (a).

we can always construct new variables $x = z \cos \phi$ and $y = z \sin \phi$, with ϕ distributed uniformly in the range $[0, 2\pi)$ which leads to $\Delta x \Delta y \geq \frac{z_c^2}{2}$. Such a distribution, however, cannot generate uncertainty bound on conjugate variables ($x, p_x = -\frac{1}{z} \sin \phi$), ($y, p_y = \frac{1}{z} \cos \phi$). A two dimensional SHO at finite temperature does exhibit noisy motion about a limit cycle $r = r_c$ in the x - y plane where the marginal distribution $P(x, y)$ is peaked. However, $P(x, y)$, as shown in Fig. 1 (b), is far from a trivial normal distribution; this feature creates bounds on $\Delta x, \Delta y$ along with bounds on $\Delta p_{x,y}$. It is worth appreciating that these distributions are created naturally as steady states of limit cycle systems under noise, an important and a ubiquitous physical system. As illustrated above, the uncertainties are not only limited to pure limit cycle systems (systems exhibiting limit cycle oscillations at $T = 0$) but also applicable to systems with an entirely different dynamics mimicking limit cycle systems under noise, that is, sharing the same steady state.

It should be noted that the validity of the uncertainty relation (18) hinges on the existence of $\langle r^{\pm 2} \rangle$ moments. For the dynamics defined in (13), $\exp(-\beta H)$ always solves the steady state Fokker-Planck equation but this probability density integrated over all space may not necessarily converge. The situation becomes even more intricate when there is conditional convergence of probability as well as moments. The logarithmic potential, an apparently simple form which shows these behaviour was considered in Sec. III C. The r^α potentials defined

in Sec. III B are free from such complications and always admit a steady state and hence uphold the uncertainty relations (18).

VI. CONCLUSION

In conclusion, we show that whenever a particle makes a noisy trajectory around a closed curve, the observables that define the phase plane would exhibit an uncertainty relation, i.e., the product of the standard deviations of these observables must be bounded from below by a positive constant. The simplest example of such a system is a limit cycle system subjected to thermal noise. In one dimension, we use the framework of canonical dissipative systems to construct limit cycles in x - p_x plane controlled by a parameter E_0 that carries the dimension of energy and show that $\Delta x \Delta p_x \geq E_0/\omega_0$, where ω_0 is the frequency of the oscillatory motion. Note that E_0/ω_0 is the simplest construct based on the parameters of the model which has the dimension of angular momentum, same as the dimension of $\Delta x \Delta p_x$. In two dimension, the dynamics of particles in a central potential does not alter the angular momentum ℓ of the system and an added radial dissipation brings the particle to follow a circular trajectory in real space (x - y plane) - in effect, limit cycles are also generated in x - p_x and y - p_y plane. Further when the radial coordinate experiences a stochastic force, the system reach a steady state having a Boltzmann distribution wrt a temperature that obeys fluctuation-dissipation relation; the angular momentum of the system, however, remains conserved. In these systems, we find a position momenta uncertainty relation in the equilibrium state: $\Delta x \Delta p_x \geq |\ell|/2$, irrespective of the nature of the radial potential (as long as $\langle r^{\pm 2} \rangle$ moments exist).

Such a thermodynamic bound of position-momenta uncertainty is not limited to limit cycle systems; we show that systems that produce a continuum of fixed points forming a closed curve, also exhibit the same when noise is added. We show it explicitly for a one dimensional system, with Hamiltonian $H = \frac{1}{2E_0} (\frac{1}{2}p_x^2 + \frac{1}{2}\omega_0^2 x^2 - E_0)^2$, which resulted in $\Delta x \Delta p_x \geq E_0/\omega_0$.

We believe, the theoretical predictions of the model can be verified in systems where particles move in a noisy trajectory around a closed curve. Once such system is an active Brownian particle in a harmonic trap in two dimension [27–33]; for very high motility they move stochastically around a circle, far away from the minimum of the potential. Another example is the chiral active particles, which naturally form noisy trajectories around a circle [34–37].

-
- [1] C. Christopher and C. Li, *Limit Cycles of Differential Equations*, Advanced Courses in Mathematics - CRM Barcelona (Birkhäuser Basel, 2007).
 [2] S. H. Strogatz, *Nonlinear Dynamics and Chaos* (CRC Press, 2018).

- [3] F. Delcomyn, Neural basis of rhythmic behavior in animals, *Science* **210**, 492–498 (1980).
 [4] M. Pals, J. H. Macke, and O. Barak, Trained recurrent neural networks develop phase-locked limit cycles in a working memory task, *PLOS Computational Biology* **20**,

- e1011852 (2024).
- [5] M. E. Gilpin, Limit cycles in competition communities, *The American Naturalist* **109**, 51 (1975).
 - [6] P. A. Abrams, R. D. Holt, and J. D. Roth, Apparent competition or apparent mutualism? shared predation when populations cycle, *Ecology* **79**, 201–212 (1998).
 - [7] D. Witthaut, F. Hellmann, J. Kurths, S. Kettemann, H. Meyer-Ortmanns, and M. Timme, Collective nonlinear dynamics and self-organization in decentralized power grids, *Reviews of Modern Physics* **94**, 10.1103/revmodphys.94.015005 (2022).
 - [8] R. Erban and H.-W. Kang, Chemical systems with limit cycles, *Bulletin of Mathematical Biology* **85**, 10.1007/s11538-023-01170-3 (2023).
 - [9] R. J. Field and R. M. Noyes, Oscillations in chemical systems. iv. limit cycle behavior in a model of a real chemical reaction, *The Journal of Chemical Physics* **60**, 1877–1884 (1974).
 - [10] A. L. Hodgkin and A. F. Huxley, A quantitative description of membrane current and its application to conduction and excitation in nerve, *The Journal of Physiology* **117**, 500–544 (1952).
 - [11] R. M. May, Limit cycles in predator-prey communities, *Science* **177**, 900–902 (1972).
 - [12] B. van der Pol, Vii.forced oscillations in a circuit with non-linear resistance. (reception with reactive triode), *The London, Edinburgh, and Dublin Philosophical Magazine and Journal of Science* **3**, 65–80 (1927).
 - [13] J. V. Carroll and R. K. Mehra, Bifurcation analysis of nonlinear aircraft dynamics, *Journal of Guidance, Control, and Dynamics* **5**, 529–536 (1982).
 - [14] T. Roenneberg, E. J. Chua, R. Bernardo, and E. Mendoza, Modelling biological rhythms, *Current Biology* **18**, R826–R835 (2008).
 - [15] C. Kurrer and K. Schulten, Effect of noise and perturbations on limit cycle systems, *Physica D: Nonlinear Phenomena* **50**, 311–320 (1991).
 - [16] S. Shmakov and P. B. Littlewood, Coalescence of limit cycles in the presence of noise, *Phys. Rev. E* **109**, 024220 (2024).
 - [17] P. Sarkar and D. S. Ray, Tuning limit cycles with a noise: Survival and collapse, *Phys. Rev. E* **109**, 034209 (2024).
 - [18] N. Mitarai, U. Alon, and M. H. Jensen, Entrainment of noise-induced and limit cycle oscillators under weak noise, *Chaos: An Interdisciplinary Journal of Nonlinear Science* **23**, 10.1063/1.4808253 (2013).
 - [19] J. M. Newby and M. A. Schwemmer, Effects of moderate noise on a limit cycle oscillator: Counterrotation and bistability, *Physical Review Letters* **112**, 10.1103/physrevlett.112.114101 (2014).
 - [20] C. Dieball and A. c. v. Godec, Direct route to thermodynamic uncertainty relations and their saturation, *Phys. Rev. Lett.* **130**, 087101 (2023).
 - [21] C. Kwon and H. K. Lee, Thermodynamic uncertainty relation for underdamped dynamics driven by time-dependent protocols, *New Journal of Physics* **24**, 013029 (2022).
 - [22] R. Sabbagh, O. Movilla Miangolarra, and T. T. Georgiou, Wasserstein speed limits for langevin systems, *Phys. Rev. Res.* **6**, 033308 (2024).
 - [23] H. Haken, Distribution function for classical and quantum systems far from thermal equilibrium, *Zeitschrift für Physik A Hadrons and nuclei* **263**, 267–282 (1973).
 - [24] F. Schweitzer, W. Ebeling, and B. Tilch, Statistical mechanics of canonical-dissipative systems and applications to swarm dynamics, *Physical Review E* **64**, 10.1103/physreve.64.021110 (2001).
 - [25] W. Ebeling and I. M. Sokolov, *Statistical Thermodynamics and Stochastic Theory of Nonequilibrium Systems* (World Scientific, 2005).
 - [26] Detailed calculations, some exact expressions and numerical results in support of our claims are given in the supplemental material.
 - [27] S. C. Takatori, R. De Dier, J. Vermant, and J. F. Brady, Acoustic trapping of active matter, *Nature Communications* **7**, 10.1038/ncomms10694 (2016).
 - [28] U. Basu, S. N. Majumdar, A. Rosso, and G. Schehr, Active brownian motion in two dimensions, *Physical Review E* **98**, 10.1103/physreve.98.062121 (2018).
 - [29] O. Dauchot and V. Démery, Dynamics of a self-propelled particle in a harmonic trap, *Physical Review Letters* **122**, 10.1103/physrevlett.122.068002 (2019).
 - [30] K. Malakar, A. Das, A. Kundu, K. V. Kumar, and A. Dhar, Steady state of an active brownian particle in a two-dimensional harmonic trap, *Physical Review E* **101**, 10.1103/physreve.101.022610 (2020).
 - [31] D. Chaudhuri and A. Dhar, Active brownian particle in harmonic trap: exact computation of moments, and re-entrant transition, *Journal of Statistical Mechanics: Theory and Experiment* **2021**, 013207 (2021).
 - [32] M. Caraglio and T. Franosch, Analytic solution of an active brownian particle in a harmonic well, *Physical Review Letters* **129**, 10.1103/physrevlett.129.158001 (2022).
 - [33] U. Nakul and M. Gopalakrishnan, Stationary states of an active brownian particle in a harmonic trap, *Physical Review E* **108**, 10.1103/physreve.108.024121 (2023).
 - [34] F. Kümmel, B. ten Hagen, R. Wittkowski, I. Buttinoni, R. Eichhorn, G. Volpe, H. Löwen, and C. Bechinger, Circular motion of asymmetric self-propelling particles, *Physical Review Letters* **110**, 10.1103/physrevlett.110.198302 (2013).
 - [35] B. ten Hagen, F. Kümmel, R. Wittkowski, D. Takagi, H. Löwen, and C. Bechinger, Gravitaxis of asymmetric self-propelled colloidal particles, *Nature Communications* **5**, 10.1038/ncomms5829 (2014).
 - [36] T. Mano, J.-B. Delfau, J. Iwasawa, and M. Sano, Optimal run-and-tumble-based transportation of a janus particle with active steering, *Proceedings of the National Academy of Sciences* **114**, 10.1073/pnas.1616013114 (2017).
 - [37] L. Caprini and U. Marini Bettolo Marconi, Active chiral particles under confinement: surface currents and bulk accumulation phenomena, *Soft Matter* **15**, 2627–2637 (2019).

Supplemental Material for “Statistical Uncertainties of Limit Cycle Systems in Langevin Bath”

Dipesh K. Singh and P. K. Mohanty*

Department of Physical Sciences, Indian Institute of Science Education and Research Kolkata, Mohanpur, 741246, India.

(Dated: February 19, 2025)

In this Supplemental Material, we give a description of the Fokker-Planck equation rewritten in a specific form (in the main text) along with its method of solution. We also show explicit calculation of partition function (Eq. (8) of the main text) for 1D limit cycle system under noise. We also provide the exact expressions of the mean energy for r^α potentials. We elaborate further on the dynamical behaviour of r^α potentials aided by linear stability analysis at $T = 0$.

I. FOKKER-PLANCK EQUATION

We will follow summation convention in this section, i.e., repeated indices are summed over. For a set of N -variable Langevin equations of the form

$$\dot{\zeta}_i = h_i(\zeta, t) + g_{ij}(\zeta, t)\xi_j(t), \quad (1)$$

with $\langle \xi_i(t) \rangle = 0$ and $\langle \xi_i(t)\xi_j(t') \rangle = 2\delta_{ij}\delta(t-t')$, the Fokker-Planck equation for the probability density $P(\zeta, t)$ is given by

$$\frac{\partial P}{\partial t} = -\frac{\partial}{\partial \zeta_i}(D_i P) + \frac{\partial^2}{\partial \zeta_i \partial \zeta_j}(D_{ij} P), \quad (2)$$

where $D_i = h_i + \frac{\partial g_{ij}}{\partial \zeta_k} g_{kj}$ and $D_{ij} = g_{ik} g_{jk}$ are the so-called drift and diffusion coefficients respectively [1].

For a noisy dynamics derived from the dynamics generated by a Hamiltonian H , as is our case, with the equations

$$\dot{x}_i = \frac{\partial H}{\partial p_i}, \quad \dot{p}_i = -\frac{\partial H}{\partial x_i} - f_i(x, p) + g_i(x, p)\xi_i(t) \quad (3)$$

with $\langle \xi_i(t) \rangle = 0$ and $\langle \xi_i(t)\xi_j(t') \rangle = 2\delta_{ij}\delta(t-t')$, the Fokker-Planck equation for probability density $P(x, p, t)$ can now be written as

$$\frac{\partial P}{\partial t} = [H, P] + \mathcal{L}P = [H, P] + \frac{\partial}{\partial p_i} \left(f_i P + \frac{\partial}{\partial p_i} (g_i P) \right), \quad (4)$$

where $[A, B] = \frac{\partial A}{\partial x_i} \frac{\partial B}{\partial p_i} - \frac{\partial A}{\partial p_i} \frac{\partial B}{\partial x_i}$ is the Poisson bracket of A and B . Corresponding to Eq. (1) in the main text, the steady state Fokker-Planck equation is given by

$$[H, P] + \frac{\partial}{\partial p_x} \left(\gamma g(H) \frac{\partial H}{\partial p_x} P + \gamma T \frac{\partial P}{\partial p_x} \right) = 0. \quad (5)$$

As mentioned in the main text, the above is solved using the ansatz $P = P(H)$. With this assumption, the Poisson bracket vanishes and using chain rule and the problem simplifies to solving $\mathcal{L}P = 0$, i.e.,

$$\frac{\partial}{\partial p_x} \left(\gamma g(H) \frac{\partial H}{\partial p_x} P + \gamma T \frac{\partial P}{\partial p_x} \frac{\partial H}{\partial p_x} \right) = 0 \quad \Rightarrow \quad \frac{\partial}{\partial p_x} \left(\gamma T \frac{\partial H}{\partial p_x} \left(\beta g(H) P + \frac{\partial P}{\partial H} \right) \right) = 0. \quad (6)$$

The above reduces to solving the equation

$$\frac{\partial P}{\partial H} + \beta g(H) P = 0 \quad (7)$$

* pkmohanty@iiserkol.ac.in

which of course has a solution given by

$$P(H) = \frac{1}{\mathcal{Z}} \exp\left(-\beta \int dH g(H)\right) \quad (8)$$

where the partition function \mathcal{Z} should be finite for P to be a valid probability density function.

Similarly, corresponding to Langevin equations

$$\dot{r} = p_r, \quad \dot{p}_r = -V'(r) + \frac{\ell^2}{r^3} - \gamma p_r + \sqrt{\gamma T} \xi(t), \quad \dot{\phi} = \frac{\ell}{r^2}, \quad (9)$$

the steady state Fokker-Planck is given by

$$[H, P] + \frac{\partial}{\partial p_r} \left(\gamma p_r P + \gamma T \frac{\partial P}{\partial p_r} \right) = 0. \quad (10)$$

Using the ansatz $P = P(H)$, and noting that $\frac{\partial H}{\partial p_r} = p_r$, we have

$$\frac{\partial}{\partial p_r} \left(\gamma p_r P + \gamma T \frac{\partial P}{\partial H} \frac{\partial H}{\partial p_r} \right) = \frac{\partial}{\partial p_r} \left(\gamma p_r \left(P + T \frac{\partial P}{\partial H} \right) \right) = 0. \quad (11)$$

Thus, $P(H) \sim \exp(-\beta H)$ solves the above equation. We demand that the probability density integrated over all space converges and hence, the partition function

$$\mathcal{Z}_\ell(\beta) = \int_0^{2\pi} d\phi \int_{-\infty}^{\infty} dp_r \int_0^{\infty} dr P(r, p_r) = \int_0^{2\pi} d\phi \int_{-\infty}^{\infty} dp_r \int_0^{\infty} dr \exp(-\beta H) = \text{finite}. \quad (12)$$

If above holds, $P(H) = \frac{e^{-\beta H}}{\mathcal{Z}_\ell(\beta)}$ is the steady state solution.

In Sec. V A of the main text, we wanted to devise a dynamics which would yield $P \sim \exp(-\beta \tilde{H})$ as the steady state. To do so, consider the set of equations

$$\dot{x} = \frac{\partial \tilde{H}}{\partial p_x}, \quad \dot{p}_x = -\frac{\partial \tilde{H}}{\partial x} - f + \sqrt{\gamma T} \xi(t) \quad (13)$$

where f is undetermined as of now. The steady state Fokker-Planck equation for above is given by

$$[\tilde{H}, P] + \frac{\partial}{\partial p_x} \left(f P + \gamma T \frac{\partial P}{\partial p_x} \right) = 0. \quad (14)$$

Using the ansatz $P = P(\tilde{H})$, the above simplifies to

$$\frac{\partial}{\partial p_x} \left(f P + \gamma T \frac{\partial P}{\partial \tilde{H}} \frac{\partial \tilde{H}}{\partial p_x} \right) = 0 \quad \Rightarrow \quad \frac{\partial}{\partial p_x} \left(\gamma \frac{\partial \tilde{H}}{\partial p_x} \left(\frac{f}{\gamma \frac{\partial \tilde{H}}{\partial p_x}} P + T \frac{\partial P}{\partial \tilde{H}} \right) \right) = 0. \quad (15)$$

Choose $f = \gamma \frac{\partial \tilde{H}}{\partial p_x}$. The above equation reduces to

$$\frac{\partial}{\partial p_x} \left(\gamma \frac{\partial \tilde{H}}{\partial p_x} \left(P + T \frac{\partial P}{\partial \tilde{H}} \right) \right) = 0 \quad (16)$$

which leads to the solution $P(H) \sim \exp(-\beta \tilde{H})$.

II. CALCULATION OF PARTITION FUNCTION

We compute the partition function (8) in the main text. We need to evaluate the integral

$$\mathcal{Z}_{E_0}(\beta) = \int_{-\infty}^{\infty} dp_x \int_{-\infty}^{\infty} dx \exp\left(-\frac{\beta}{2E_0} \left(\frac{p_x^2}{2} + \frac{kx^2}{2} - E_0 \right)^2\right). \quad (17)$$

This is best done using a coordinate transform

$$x = \sqrt{\frac{2}{k}} r \cos \phi, \quad p_x = \sqrt{2} r \sin \phi \quad \Rightarrow \quad dx dy = \frac{2r}{\sqrt{k}} dr d\phi. \quad (18)$$

The partition function thus becomes

$$\mathcal{Z}_{E_0}(\beta) = \frac{2}{\sqrt{k}} \int_0^{2\pi} d\phi \int_0^\infty dr r \exp\left(-\frac{\beta}{2E_0}(r^2 - E_0)^2\right) = \sqrt{\frac{2E_0}{k\beta}} \pi^{3/2} \left(1 + \operatorname{erf}\left(\sqrt{\frac{\beta E_0}{2}}\right)\right). \quad (19)$$

III. CALCULATION OF RADIAL MOMENTS FOR STEADY STATES OF CENTRAL POTENTIALS

For the distribution $e^{-\beta H}$ with $H = p_r^2/2 + \ell^2/2r^2 + V(r)$, the radial moments for $n \geq 0$ are given by

$$\langle r^n \rangle = \frac{\int_0^\infty dr r^n \exp(-\beta \tilde{V}(r))}{\int_0^\infty dr \exp(-\beta \tilde{V}(r))}; \quad \tilde{V}(r) = \frac{\ell^2}{2r^2} + V(r). \quad (20)$$

$\tilde{V}(r)$ is the effective radial potential as defined earlier. In the $T \rightarrow 0$ limit, (equivalently, $\beta \rightarrow \infty$), the value of the integral is dominated by the strongest minimum. Let r_c denote the radius of the limit cycle corresponding to this minimum. Performing the saddle-point approximation around $r = r_c$, the integral becomes

$$\langle r^n \rangle \sim \frac{\int_0^\infty dr r^n \exp\left(-\frac{\beta \tilde{V}''(r_c)}{2}(r - r_c)^2\right)}{\int_0^\infty dr \exp\left(-\frac{\beta \tilde{V}''(r_c)}{2}(r - r_c)^2\right)} = \frac{\int_{-r_c}^\infty dr (r + r_c)^n \exp\left(-\frac{\beta \tilde{V}''(r_c)r^2}{2}\right)}{\int_{-r_c}^\infty dr \exp\left(-\frac{\beta \tilde{V}''(r_c)r^2}{2}\right)}. \quad (21)$$

The above Gaussian can be integrated in terms of confluent hypergeometric function ${}_1F_1(a; b; z)$ and Gamma function. The integral evaluates to

$$\langle r^n \rangle \sim \frac{b^{-\frac{n}{2}} \left(\Gamma\left(\frac{n+1}{2}\right) {}_1F_1\left(-\frac{n}{2}; \frac{1}{2}; -r_c^2 b\right) + r_c n \sqrt{b} \Gamma\left(\frac{n}{2}\right) {}_1F_1\left(\frac{1-n}{2}; \frac{3}{2}; -r_c^2 b\right) \right)}{\sqrt{\pi} \left(\operatorname{erf}\left(r_c \sqrt{b}\right) + 1 \right)}; \quad b = \frac{\beta \tilde{V}''(r_c)}{2}. \quad (22)$$

The asymptotic form of ${}_1F_1(p; q; z)$ as $z \rightarrow -\infty$, when $\Gamma(q - p)$ is finite is given by

$${}_1F_1(p; q; z) \sim \frac{\Gamma(q)}{\Gamma(q - p)} (-z)^{-p}. \quad (23)$$

Finally taking the limit $\beta \rightarrow \infty$ (equivalently, $b \rightarrow \infty$),

$$\langle r^n \rangle \sim \frac{b^{-n/2}}{2\sqrt{\pi}} \left(\frac{\Gamma\left(\frac{n+1}{2}\right)\Gamma\left(\frac{1}{2}\right)r_c^n b^{n/2}}{\Gamma\left(\frac{n+1}{2}\right)} + \frac{n\Gamma\left(\frac{n}{2}\right)\Gamma\left(\frac{3}{2}\right)r_c^n b^{n/2}}{\Gamma\left(\frac{n+2}{2}\right)} \right) \quad (24)$$

which simplifies to

$$\langle r^n \rangle (\beta \rightarrow \infty) = r_c^n. \quad (25)$$

IV. LINEAR STABILITY ANALYSIS

We perform linear stability analysis around the limit cycle generated by dynamics (9) at $T = 0$ to get an idea about the time scale of decay of small perturbation from the limit cycle trajectory. The dynamics at $T = 0$ is given by

$$\dot{r} = p_r, \quad \dot{p}_r = -\tilde{V}'(r) - \gamma p_r, \quad \dot{\phi} = \frac{\ell}{r^2}, \quad (26)$$

where we have used the effective radial potential $\tilde{V}(r) = \ell^2/2r^2 + V(r)$. Consider small perturbations $\delta r, \delta p_r$ and $\delta\phi$ about the limit cycle at r_c . Considering terms only first order in these perturbations, we get

$$\frac{d}{dt} \begin{pmatrix} \delta r \\ \delta p_r \\ \delta\phi \end{pmatrix} = \begin{pmatrix} 0 & 1 & 0 \\ -\tilde{V}''(r_c) & -\gamma & 0 \\ -\frac{2\ell}{r_c^3} & 0 & 0 \end{pmatrix} \begin{pmatrix} \delta r \\ \delta p_r \\ \delta\phi \end{pmatrix}. \quad (27)$$

The eigenvalues and the corresponding eigenvectors of the above stability matrix are

$$\lambda_0 = 0, \quad \lambda_{\pm} = -\frac{\gamma}{2} \pm \frac{\sqrt{\gamma^2 - 4\tilde{V}''(r_c)}}{2} \quad \text{with} \quad \mathbf{v}_{\lambda_0} = \begin{pmatrix} 0 \\ 0 \\ 1 \end{pmatrix}, \quad \mathbf{v}_{\lambda_{\pm}} = \begin{pmatrix} -\frac{r_c^3}{2\ell} \lambda_{\pm} \\ -\frac{r_c^3}{2\ell} \lambda_{\pm}^2 \\ 1 \end{pmatrix}. \quad (28)$$

We therefore have

$$\begin{pmatrix} \delta r \\ \delta p_r \\ \delta\phi \end{pmatrix} (t) = c_0 \mathbf{v}_{\lambda_0} + c_+ e^{t\lambda_+} \mathbf{v}_{\lambda_+} + c_- e^{t\lambda_-} \mathbf{v}_{\lambda_-}. \quad (29)$$

In case of small damping, such that $\gamma^2 - 4\tilde{V}''(r_c) < 0$, we get an oscillatory decay of $\delta r(t)$ and $\delta p_r(t)$ to 0 with a time scale $2/\gamma$. In case of large damping, such that $\gamma^2 - 4\tilde{V}''(r_c) \geq 0$, we have an exponential decay of $\delta r(t)$ and $\delta p_r(t)$ to 0 with the time scales given by λ_{\pm}^{-1} . The time scale obtained is roughly the relaxation time of $\langle r(t) \rangle$ to steady state at small T as shown in Fig. 1 and 2. In fact, the feature of oscillatory decay for smaller values of γ and exponential decay for larger values of γ according to the conditions mentioned here is also preserved.

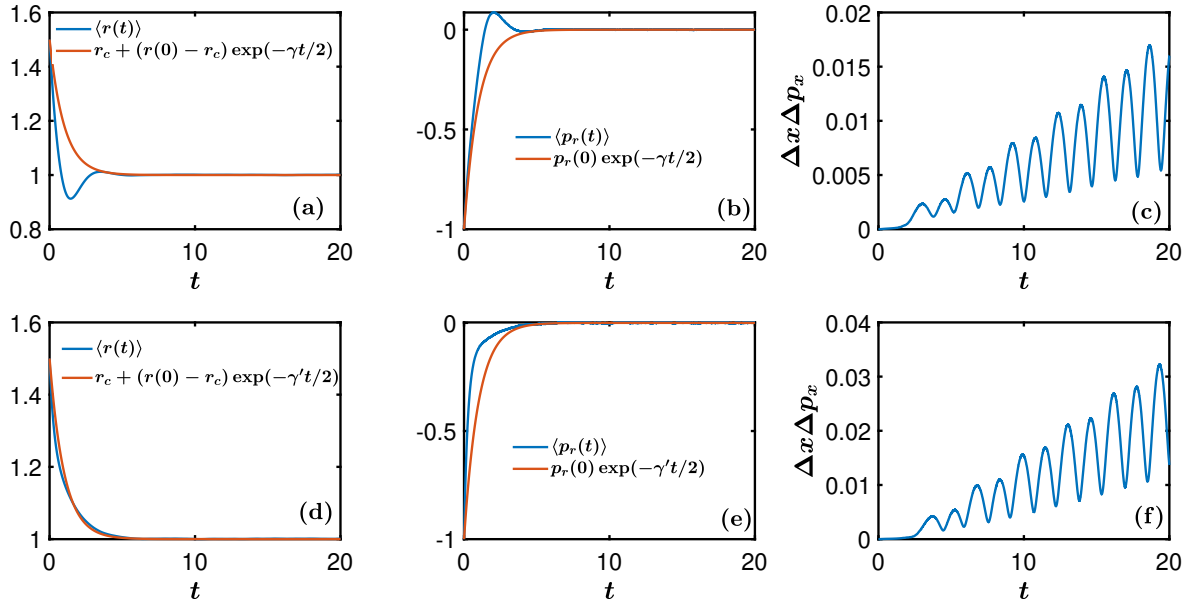


FIG. 1. Simulations for $V(r) = kr$ potential ($\alpha = 1$) at $T = 10^{-3}$ with $k = \ell = 1$. (a), (b), (c): here $\gamma = 2$ which results in the oscillatory decay of $\langle r(t) \rangle$ and $\langle p_r(t) \rangle$. The data is compared with the only time scale $\gamma = 2$. (d), (e), (f): here $\gamma = 4$ which results in an exponential decay with two time scales. The data is compared with the dominating time-scale $\gamma' = 2$. In both cases, however, the oscillatory behaviour prevails in the evolution of uncertainties, as can be seen in $\Delta x \Delta p_x$ in (c) and (f).

The dynamics (9) at $T = 0$ can be expressed in Cartesian coordinates using the relations

$$x = r \cos \phi, \quad y = r \sin \phi, \quad p_x = p_r \cos \phi - \frac{\ell}{r} \sin \phi, \quad p_y = p_r \sin \phi + \frac{\ell}{r} \cos \phi. \quad (30)$$

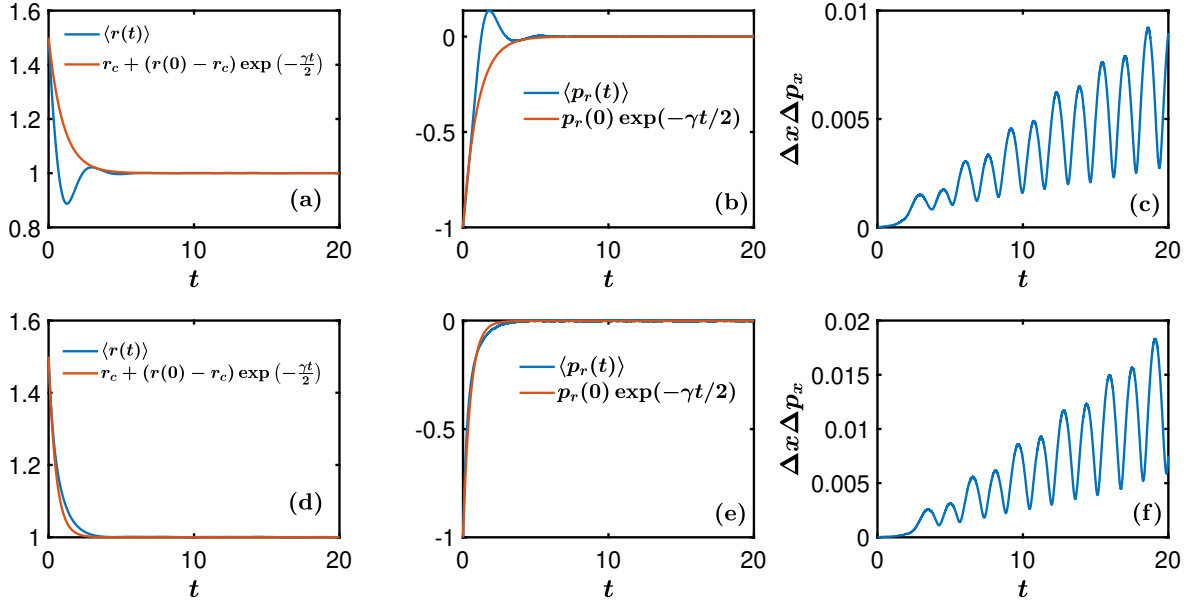


FIG. 2. Simulations for 2D SHO potential ($\alpha = 2$) at $T = 10^{-3}$ with $k = \ell = 1$. (a),(b),(c): here $\gamma = 2$ which results in oscillatory decay of $\langle r(t) \rangle$ and $\langle p_r(t) \rangle$. (d), (e), (f): here $\gamma = 4$ which shows exponential decay. This is the marginal case where both eigenvalues are same. In both cases, oscillatory behaviour still prevails in the uncertainties, as can be seen in $\Delta x \Delta p_x$ in (c) and (f).

Using above, we get

$$\begin{aligned} \dot{x} &= p_x, & \dot{p}_x &= -x \left(\frac{V'(r)}{\sqrt{x^2 + y^2}} + \gamma \frac{x p_x + y p_y}{x^2 + y^2} \right) \\ \dot{y} &= p_y, & \dot{p}_y &= -y \left(\frac{V'(r)}{\sqrt{x^2 + y^2}} + \gamma \frac{x p_x + y p_y}{x^2 + y^2} \right) \end{aligned} \quad (31)$$

where prime denotes differentiation wrt r and $r = \sqrt{x^2 + y^2}$. Note that on the limit cycle, $r = r_c$ and $p_r = 0$. We consider $V(r) = kr^\alpha/\alpha$; $\alpha > 0$ potentials. For simplicity consider $\ell = k = 1$ such that $r_c = 1$. For this case, the linear stability analysis yields the following system of equations. We denote $\sin \phi$ as s and $\cos \phi$ as c respectively.

$$\frac{d}{dt} \begin{pmatrix} \delta x \\ \delta p_x \\ \delta y \\ \delta p_y \end{pmatrix} = \begin{pmatrix} 0 & 1 & 0 & 0 \\ (\alpha - 2)s^2 - \alpha + \gamma sc + 1 & -\gamma c^2 & -c((\alpha - 2)s + \gamma c) & -\gamma cs \\ 0 & 0 & 0 & 1 \\ s((2 - \alpha)c + \gamma s) & -\gamma cs & -s((\alpha - 2)s + \gamma c) - 1 & -\gamma s^2 \end{pmatrix} \begin{pmatrix} \delta x \\ \delta p_x \\ \delta y \\ \delta p_y \end{pmatrix} \quad (32)$$

The stability matrix above is a function of time owing to the time dependence of ϕ . In fact, here, we have $\dot{\phi} = 1$ so $\phi(t) = t + \phi_0$ on the limit cycle with ϕ_0 being a constant fixed by the initial conditions. The above system of equations cannot be integrated analytically and hence, it is not possible to get some analytical form of time scale of decay of perturbations. If one considers a fixed ϕ , the eigenvalues and eigenvectors will be different for different times and hence, the linear stability analysis does not shed any light on the behaviour of the system. In fact, for some values of ϕ the eigenvalues indicate a diverging solution which is unphysical in context of a stable limit cycle. The same problems arise even when we work with an averaged ϕ in the stability matrix. Thus, linear stability analysis which gave us reasonable estimate of the relaxation of $\langle r(t) \rangle$, $\langle p_r(t) \rangle$, fails to capture the oscillatory behaviour of $\langle x(t) \rangle$, $\langle y(t) \rangle$ and $\langle p_{x,y}(t) \rangle$ at low T .

V. DYNAMICAL UNCERTAINTIES

We illustrate some additional features of the dynamics for $V(r) = kr^\alpha/\alpha$ potentials. As one would expect, the relaxation time, τ decreases with increasing T . We show this feature for $\alpha = 2$ in Fig. 3. $\langle r(t) \rangle$ relaxes much faster than any of $\langle x(t)^n \rangle$, $\langle y(t)^n \rangle$, $\langle p_x(t)^n \rangle$ and $\langle p_y(t)^n \rangle$ where $n \geq 1$. This has been shown in Fig. 4 for $\alpha = 2$.

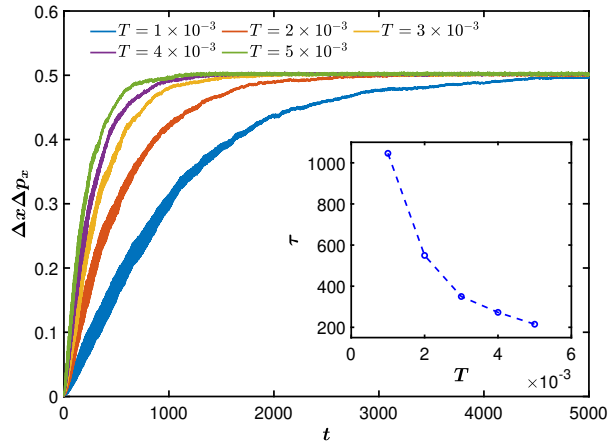


FIG. 3. Variation of $\Delta x \Delta p_x$ with t for different T . The simulations have been performed for $\alpha = 2$ with $\gamma = 2$ and $k = 1 = \ell$ for $T = (1, 2, 3, 4, 5) \times 10^{-3}$ and τ has been found out by fitting the curves to $\frac{1}{2}(1+T)(1 - \exp(-t/\tau))$ where $\frac{1}{2}(1+T)$ is the steady state value of $\Delta x \Delta p_x$ for $\alpha = 2$.

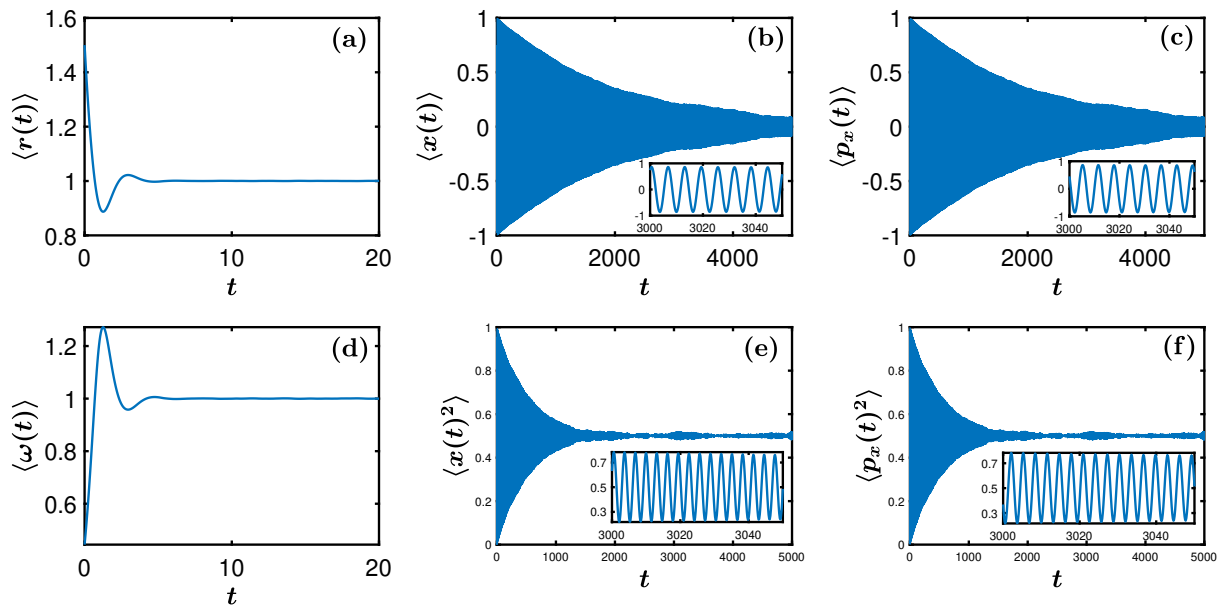


FIG. 4. The above has been obtained from simulation of $\alpha = 2$, that is, SHO potential at $T = 10^{-3}$ and $\gamma = 2$, $k = \ell = 1$. (a) and (d) show the quick relaxation of $\langle r(t) \rangle$ and $\langle \dot{\phi} = \omega(t) \rangle$ to steady state. On the other hand, $\langle x(t) \rangle$, $\langle p_x(t) \rangle$, $\langle x(t)^2 \rangle$ and $\langle p_x(t)^2 \rangle$ have a much longer relaxation time scale as shown in (b), (c), (e) and (f) respectively. The insets show the prevailing oscillatory behaviour of these moments.

VI. EXPRESSIONS OF AVERAGE ENERGY FOR POWER-LAW CENTRAL POTENTIALS

The expressions for $\langle E \rangle$ and $\langle E_{\text{rot}} \rangle$ for $V(r) = \frac{kr^\alpha}{\alpha}$ are given below.

α	$\langle E_{\text{rot}} \rangle$	$\langle E \rangle$
1	$\frac{\beta^2 k^2 \ell^2 G_{0,3}^{3,0} \left(\frac{1}{8} k^2 \ell^2 \beta^3 \mid -\frac{1}{2}, 0, 0 \right)}{8 G_{0,3}^{3,0} \left(\frac{1}{8} k^2 \ell^2 \beta^3 \mid 0, \frac{1}{2}, 1 \right)}$	$\frac{3}{8\beta} \left(4 + \frac{\beta^3 k^2 \ell^2 G_{0,3}^{3,0} \left(\frac{1}{8} k^2 \ell^2 \beta^3 \mid -\frac{1}{2}, 0, 0 \right)}{G_{0,3}^{3,0} \left(\frac{1}{8} k^2 \ell^2 \beta^3 \mid 0, \frac{1}{2}, 1 \right)} \right)$
1.5	$\frac{3 G_{0,7}^{7,0} \left(\frac{3.57 k^4 \ell^6 \beta^7}{10^6} \mid 0, \frac{1}{6}, \frac{1}{4}, \frac{1}{2}, \frac{1}{2}, \frac{3}{4}, \frac{5}{6} \right)}{\beta G_{0,7}^{7,0} \left(\frac{3.57 k^4 \ell^6 \beta^7}{10^6} \mid -\frac{1}{6}, 0, \frac{1}{6}, \frac{1}{4}, \frac{1}{2}, \frac{1}{2}, \frac{3}{4} \right)}$	$\frac{2.5 \beta^6 k^4 \ell^6 G_{0,7}^{7,0} \left(\frac{3.57 k^4 \ell^6 \beta^7}{10^6} \mid -\frac{7}{6}, -\frac{5}{6}, -\frac{3}{4}, -\frac{1}{2}, -\frac{1}{2}, -\frac{1}{4}, 0 \right)}{10^5 G_{0,7}^{7,0} \left(\frac{3.57 k^4 \ell^6 \beta^7}{10^6} \mid -\frac{1}{6}, 0, \frac{1}{6}, \frac{1}{4}, \frac{1}{2}, \frac{1}{2}, \frac{3}{4} \right)}$
2	$\frac{\sqrt{k} \ell }{2}$	$\frac{1}{\beta} + \sqrt{k} \ell $
2.5	$\frac{5 G_{0,9}^{9,0} \left(\frac{k^4 \ell^{10} \beta^9}{10^9} \mid 0, \frac{1}{10}, \frac{1}{4}, \frac{3}{10}, \frac{1}{2}, \frac{1}{2}, \frac{7}{10}, \frac{3}{4}, \frac{9}{10} \right)}{\beta G_{0,9}^{9,0} \left(\frac{k^4 \ell^{10} \beta^9}{10^9} \mid -\frac{1}{10}, 0, \frac{1}{10}, \frac{1}{4}, \frac{3}{10}, \frac{1}{2}, \frac{1}{2}, \frac{7}{10}, \frac{3}{4} \right)}$	$\frac{9 k^4 \ell^{10} \beta^8 G_{0,9}^{9,0} \left(\frac{k^4 \ell^{10} \beta^9}{10^9} \mid -\frac{11}{10}, -\frac{9}{10}, -\frac{3}{4}, -\frac{7}{10}, -\frac{1}{2}, -\frac{1}{2}, -\frac{3}{10}, -\frac{1}{4}, 0 \right)}{10^9 G_{0,9}^{9,0} \left(\frac{k^4 \ell^{10} \beta^9}{10^9} \mid -\frac{1}{10}, 0, \frac{1}{10}, \frac{1}{4}, \frac{3}{10}, \frac{1}{2}, \frac{1}{2}, \frac{7}{10}, \frac{3}{4} \right)}$
3	$\frac{3 G_{0,5}^{5,0} \left(\frac{k^2 \ell^6 \beta^5}{7776} \mid 0, \frac{1}{6}, \frac{1}{2}, \frac{1}{2}, \frac{5}{6} \right)}{\beta G_{0,5}^{5,0} \left(\frac{k^2 \ell^6 \beta^5}{7776} \mid -\frac{1}{6}, 0, \frac{1}{6}, \frac{1}{2}, \frac{1}{2} \right)}$	$\frac{5 k^2 \ell^6 \beta^4 G_{0,5}^{5,0} \left(\frac{k^2 \ell^6 \beta^5}{7776} \mid -\frac{7}{6}, -\frac{5}{6}, -\frac{1}{2}, -\frac{1}{2}, 0 \right)}{7776 G_{0,5}^{5,0} \left(\frac{k^2 \ell^6 \beta^5}{7776} \mid -\frac{1}{6}, 0, \frac{1}{6}, \frac{1}{2}, \frac{1}{2} \right)}$

where $G_{p,q}^{m,n} \left(z \mid \begin{matrix} a_1, \dots, a_p \\ b_1, \dots, b_q \end{matrix} \right)$ is the Meijer G-function. Average potential energy, $\langle V(r) \rangle$ can be calculated using $\langle V(r) \rangle = \langle E \rangle - \langle E_{\text{rot}} \rangle - T/2$.

[1] H. Risken, The Fokker-Planck Equation: Methods of Solution and Applications (Springer Berlin Heidelberg, 1996)